Kaon and pion production in central Au+Au collisions at $\sqrt{s_{NN}}$ = 62.4 GeV[☆]

I.C.Arsene[*,k], I.G.Bearden[f], D.Beavis[a], S.Bekele[j,1], C.Besliu[i], B.Budick[e], H.Bøggild[f], C.Chasman[a], C.H.Christensen[f], P.Christiansen[f,4], H.H.Dalsgaard[f], R.Debbe[a], J.J.Gaardhøje[f], K.Hagel[g], H.Ito[a], A.Jipa[i], E.B.Johnson[j,2], C.E.Jørgensen[f,6], R.Karabowicz[d], N.Katrynska[d], E.J.Kim[j,3], T.M.Larsen[f], J.H.Lee[a], G.Løvhøiden[k], Z.Majka[d], M.J.Murray[j], J.Natowitz[g], B.S.Nielsen[f], C.Nygaard[f], D.Pal[j], A.Qviller[k], F.Rami[1], C.Ristea[f], O.Ristea[i], D.Röhrich[h], S.J.Sanders[j], P.Staszel[d], T.S.Tveter[k], F.Videbæk[a,8], R.Wada[g], H.Yang[h,7], Z.Yin[h,5], and I.S.Zgura[c]

[a]*Brookhaven National Laboratory, Upton, New York, USA*
[b]*Institut Pluridisciplinaire Hubert Curien et Université Louis Pasteur, Strasbourg, France*
[c]*Institute of Space Science,Bucharest-Magurele, Romania*
[d]*M. Smoluchowski Inst. of Physics, Jagiellonian University, Krakow, Poland*
[e]*New York University, New York, USA,*
[f]*Niels Bohr Institute, University of Copenhagen, Copenhagen, Denmark*
[g]*Texas A&M University, College Station, Texas, USA*
[h]*University of Bergen, Department of Physics and Technology, Bergen, Norway*
[i]*University of Bucharest, Romania*
[j]*University of Kansas, Lawrence, Kansas, USA*
[k]*University of Oslo, Department of Physics, Oslo, Norway*

Abstract

Invariant p_T spectra and rapidity densities covering a large rapidity range ($-0.1 < y < 3.5$) are presented for $\pi^{\pm}$ and $K^{\pm}$ mesons from central Au+Au collisions at $\sqrt{s_{NN}}$ = 62.4 GeV. The mid-rapidity yields of meson particles relative to their anti-particles are found to be close to unity ($\pi^-/\pi^+ \sim 1$, $K^-/K^+ \sim 0.85$) while the anti-proton to proton ratio is $\bar{p}/p \sim 0.45$. The rapidity dependence of the π^-/π^+ ratio is consistent with a small increase towards forward rapidities while the K^-/K^+ and $\bar{p}/p$ ratios show a steep decrease to ~ 0.3 for kaons and 0.024 for protons at $y \sim 3$. It is observed that the kaon production relative to its anti-particle and pion production in the wide rapidity and energy ranges show an apparent universal behavior commonly driven by baryo-chemical potentials deduced from the $\bar{p}/p$ ratio.

Key words: heavy ion collisions, strangeness enhancement, baryon chemical potential
PACS: 25.75q

Introduction

As the collision energy has increased with the advent of newer relativistic heavy-ion accelerators, from AGS energies ($\sqrt{s_{NN}} \leq 4.9$ GeV) to those achieved with the SPS ($\sqrt{s_{NN}} \leq 17.3$ GeV) and recently with RHIC ($\sqrt{s_{NN}} \leq 200$ GeV), the fireball generated in heavy-ion collisions has been found to evolve from one that is baryon rich to one dominated by mesons [1, 2, 3, 4]. This change is evident in the rapid increase in the central rapidity densities of emitted pions and kaons and the simultaneous change of the net-baryon peak, which gradually moves from mid-rapidity (AGS and SPS) [5, 6] towards forward rapidity (RHIC) [7], leaving a relatively net-baryon poor region at mid-rapidity at the highest RHIC energy.

At AGS energies, the observed ratio of produced strange particles to the number of produced pions in A+A collisions is larger than that measured in either p+p or p+A collisions and this ratio increases significantly with beam energy [2, 8, 9]. This behavior is understood in cascade models as arising from hadronic rescatterings involving heavy baryon resonances [10, 11]. In the SPS energy range it is conjectured [12] that the nuclear fireball undergoes a phase transition from bound hadronic matter to a deconfined quark-gluon plasma state (QGP). This conjecture is supported by the observation that excitation functions of the K^+/π^+, Λ/π, and Ξ^-/π ratios at mid-rapidity are found to peak around $\sqrt{s_{NN}}$ = 7.6 GeV [13] and then decrease slightly with increasing energy. The energy

☆The BRAHMS Collaboration
*Corresponding Author. *e-mail: i.c.arsene@fys.uio.no*(I.C.Arsene)
Present Address: ExtreMe Matter Institute EMMI, GSI Helmholtzzentrum für Schwerionenforschung GmbH, Darmstadt, Germany
[1]Present Address: Dept of Physics, Tennessee Tech University,Cookeville, Tennessee
[2]Present address: Radiation Monitoring Devices, Cambridge, MA, USA
[3]Present address: Division of Science Education, Chonbuk National University, Jeonju, Korea
[4]Present Address: Div. of Experimental High-Energy Physics, Lund University, Lund, Sweden
[5]Present Address: Institute of Particle Physics, Huazhong Normal University,Wuhan,China
[6]Present Address: Risø National Laboratory, Denmark
[7]Present Address: Physics Institute, University of Heidelberg, Heidelberg, Germany
[8]Spokesperson *e-mail: videbaek@bnl.gov*

dependence of other observables, like the onset of a plateau for the kaon spectra inverse slope parameter and a kink in the 4π pion yields normalized to the number of participant nucleons $\langle\pi\rangle/N_{part}$, is also used to support the transition to a deconfined phase at $\sqrt{s_{NN}}$ = 7.6 GeV [13]. The gross features of the K/π excitation function can be described in theoretical models but additional features are needed to describe the data quantitatively. Phenomenologically motivated thermal models can explain this behavior with the assumption of a QGP formed in the early stages of the collision [12]. The K^-/π^- ratio has a monotonically increasing energy dependence and is always lower than the K^+/π^+ ratio because of the larger share of strange quarks which form baryons (mainly Λ's) [13]. From the top SPS energy to the top RHIC energy the K^+/π^+ ratio at mid-rapidity is fairly constant, suggesting that the nuclear medium reaches equilibrium with respect to the production of strange quarks [4].

We present invariant p_T spectra of pions and kaons in central ($0-10\%$) Au+Au collisions at $\sqrt{s_{NN}}$ = 62.4 GeV measured by the BRAHMS spectrometers[14]. At this energy it is possible by varying the spectrometer angles to achieve an overlap in terms of the baryo-chemical potential (as reflected in the $\bar{p}/p$ ratio) of the RHIC and higher energy SPS results. The data cover the rapidity interval $-0.1 < y < 3.5$, which extends well towards the beam rapidity (y_{beam} = 4.2). Total yields deduced from the spectra are used to calculate particle ratios that can be compared to the lower energy SPS results and to theoretical models. The large rapidity coverage allows very different nuclear media to be probed: at mid-rapidity the fireball is dense and with high anti-hadron/hadron ratios ($\pi^-/\pi^+ \sim 1$, $K^-/K^+ \sim 0.85$, $\bar{p}/p \sim 0.45$), while at forward rapidity, in the fragmentation region, we observe a net-baryon rich medium with ~ 4 times smaller meson densities and a 20 times smaller $\bar{p}/p$ ratio. By covering a large interval for important physical parameters (*e.g.* rapidity, particle density, net-baryon density, baryo-chemical potential), these measurements will provide additional constraints to those models that support the conjecture of a phase transition to quark-gluon plasma.

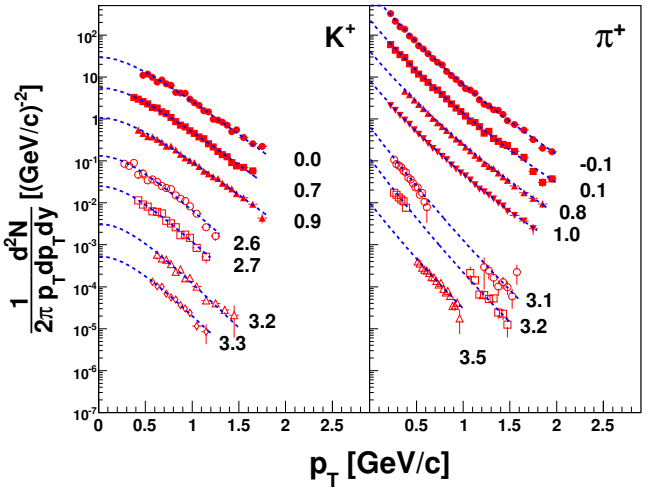

Figure 1: Spectra for K^+ (left) and π^+ (right) from 0-10% central Au+Au collisions at $\sqrt{s_{NN}}$ = 62.4 GeV in selected rapidity slices. Each spectrum is multiplied with a factor of 0.2^n for better visibility, with n = 0,1,2,... . The fits are m_T exponentials for kaons and p_T power laws for pions. The numbers on the plot indicate the rapidity corresponding to each spectrum. The error bars represent statistical errors.

Experimental setup and data analysis

The BRAHMS experiment consists of global event characterization detectors and two spectrometer arms. Collision centrality is determined using a hybrid array of Si strip detectors and plastic scintillator tiles located about the nominal interaction point. The Mid-Rapidity Spectrometer (MRS) and the Forward Spectrometer (FS) each covers a relatively small solid angle but can be rotated in the horizontal plane so as to achieve angular coverage from 90° to 2.3°. For the present studies, the MRS spectrometer was positioned at 90°, 45° and 40° and the FS at 6°, 4° and 3° at a few magnetic field settings. The length of the 62.4 GeV Au+Au run was relatively short, so data was recorded only at a few settings.

Particle identification (PID) is achieved in both spectrometers using time-of-flight walls (TOFW in MRS and H2 in FS) and additionally in the FS a ring imaging Cherenkov detector (RICH). A detailed description of the technical capabilities of the experimental setup can be found in references [15] and [16]. The identification of charged pions and kaons with the time-of-flight detectors was done by using cuts in (m^2, p) space, where $m^2 = p^2(t^2_{TOF}/L^2 - 1/c^2)$ is determined for a given momentum p by using the time of flight (t_{TOF}) and the track path length(L). Momentum dependent three-σ cuts about the mean m^2 of a given species were applied with the additional condition that the level of contamination from other species at a given m^2 and p is limited to 5% inside the cut. Clean $\pi - K$ separation is achieved up to momenta of 1.5 GeV/c in the MRS and 3 GeV/c in the FS. For higher momenta the 3σ curves overlap and the contamination condition gives asymmetrical cuts in the (m^2, p) space, necessitating the use of momentum dependent cuts and corrections. For the TOFW, the momentum dependent PID correction ranges from 0 at 1.5 GeV/c up to 20% for pions and 50% for kaons at 2.2 GeV/c. In H2, the same correction ranges from 0 at 3 GeV/c to 10% and 80% at 4.5 GeV/c for pions and kaons, respectively. In the FS, the RICH was used to identify pions and kaons at higher momenta. The pions are separated from kaons by comparing the reconstructed Cherenkov ring radii for momenta with the calculated value for pions in the momentum range of 2.5 to 20 GeV/c. Kaons are identified by the RICH above 10 GeV/c where the RICH efficiency saturates at a value of 97% [16]. Between 4.5 GeV/c and 9 GeV/c an indirect method labels as kaons particles, which give no signal in the RICH, and which are not identified as protons in H2. The contamination of kaons with pions unresolved in RICH and protons unresolved in H2 depends on momentum and on relative particle abundances. For K^- the contaminant contribution is estimated to be almost constant at 20% whereas for K^+ it varies from 14% to 40%.

Invariant differential yields, $\frac{1}{2\pi}\frac{d^2N}{p_T dp_T dy}$, were constructed for each spectrometer setting and were corrected for geometrical

Table 1: dN/dy values for charged pions as a function of rapidity. The given errors are statistical only. Fiducial yield is the integrated yield covered by the experimental p_T range.

y	dN/dy power law			dN/dy m_T expo			fiducial yields	
	π^+	π^-	p_T [GeV/c]	π^+	π^-	p_T [GeV/c]	π^+	π^-
-0.20≤y≤0.00	224.0±2.7	232.4±2.9	0.20 - 2.00	195.8±2.2	202.1±2.4	0.20 - 1.00	167.9±2.1	170.4±2.3
0.00≤y≤0.20	231.9±3.2	233.7±2.9	0.20 - 2.00	202.7±2.7	203.6±2.3	0.20 - 1.00	171.7±2.5	171.7±2.1
0.70≤y≤0.90	209.7±2.1	213.1±2.2	0.35 - 1.90	180.7±1.3	182.4±1.4	0.35 - 1.00	99.7±0.6	100.3±0.6
0.90≤y≤1.10	205.5±1.9	214.3±1.9	0.20 - 1.80	178.6±1.2	185.4±1.1	0.20 - 1.00	151.1±1.7	135.9±0.9
3.05≤y≤3.15	57.1±1.9	68.6±3.2	0.25 - 1.60	49.9±0.9	52.2±0.8	0.25 - 1.60	22.4±0.5	24.8±0.5
3.15≤y≤3.25	49.2±1.4	60.5±2.0	0.25 - 1.50	45.8±1.1	53.1±1.2	0.25 - 1.50	11.0±0.4	8.3±0.2
3.40≤y≤3.60	24.8±2.0	24.3±3.7	0.50 - 1.00	20.3±1.2	19.9±1.0	0.50 - 1.00	4.8±0.1	4.9±0.1

Table 2: dN/dy values for charged kaons as a function of rapidity. The errors are statistical only. Fiducial yield is the integrated yield covered by the experimental p_T range

y	dN/dy m_T expo			dN/dy Boltzmann			fiducial yields	
	K^+	K^-	p_T [GeV/c]	K^+	K^-	p_T [GeV/c]	K^+	K^-
-0.15≤y≤0.15	35.64±0.92	30.35±0.79	0.45 - 1.90	33.61±0.82	28.58±0.75	0.45 - 1.90	19.51±0.51	16.58±0.46
0.60≤y≤0.80	33.44±0.44	27.53±0.40	0.35 - 1.80	31.57±0.42	25.95±0.38	0.35 - 1.90	23.89±0.34	15.03±0.21
0.80≤y≤1.00	32.22±0.64	26.74±0.53	0.40 - 1.80	30.07±0.52	26.74±0.53	0.40 - 1.80	19.08±0.39	11.71±0.22
2.55≤y≤2.65	15.15±0.38	8.76±0.27	0.25 - 1.30	14.77±0.37	8.57±0.26	0.25 - 1.30	11.50±0.39	6.60±0.21
2.65≤y≤2.75	13.96±0.38	8.16±0.25	0.35 - 1.20	13.45±0.37	7.91±0.24	0.35 - 1.20	6.57±0.18	4.74±0.14
3.15≤y≤3.25	8.07±0.55	2.89±0.29	0.60 - 1.50	7.53±0.51	2.71±0.27	0.60 - 1.50	2.44±0.12	0.84±0.06
3.25≤y≤3.35	6.77±0.28	2.34±0.14	0.50 - 1.20	6.34±0.26	2.20±0.14	0.50 - 1.20	1.83±0.07	0.75±0.04

acceptance, tracking and PID efficiency, contamination, in-flight weak decays and multiple scattering effects by using a Monte Carlo calculation simulating the geometry and tracking of the BRAHMS detector system. The feed-down correction for charged pions originating in the weak decays of K^0_S and Λ was applied as described in reference [4] and amounts to 5% of the measured yield in MRS settings and 7% in FS settings. The feed-down correction was applied directly to the p_T integrated rapidity densities. By merging all of the spectrometer magnet settings, invariant p_T spectra were extracted in several rapidity intervals and fitted with different functions in order to extract the integrated yields (see Fig. 1). We estimate the point-to-point systematic errors to be ≤5% while the systematic errors from normalization, tracking efficiencies and other corrections to be ∼8%. The spectrometer acceptances allow measurements down to p_T = 0.2 GeV/c for pions and p_T = 0.25 GeV/c for kaons, with the absence of lower momentum data contributing to the systematic errors for the integral yield. This uncertainty is larger for pions because the average p_T for this species is lower than that observed for kaons. In order to estimate the extrapolation uncertainty, we used both a power law distribution of the form $A(1 + p_T/p_0)^{-B}$ and an m_T exponential function to fit the pion spectra. Of these two, the power law distribution gives the best fit to the experimental results over the observed momentum range, and for very low p_T ($p_T < 0.1$ GeV/c) agrees with the measurements made by the PHOBOS collaboration at $y = 0.8$ [17]. For the m_T exponential function the fit range is limited to $p_T < 1$ GeV/c. The kaon spectra are equally well described by an m_T exponential function, $A\exp(-m_T/T)$, and by a Boltzmann distribution.

Results and discussion

The resulting p_T integrated yields, dN/dy, for pion and kaons are shown in Tables 1 and 2. The dN/dy distributions, taking the statistically weighted average of the two functional forms used in fitting each species, are shown in the upper panel of Fig. 2. The horizontal error bars indicate the width of the rapidity slices and the vertical error bars, smaller than the marker size, are statistical errors. The square brackets below and above each data point indicate the dN/dy values extracted with the employed functionals (see Tables 1 and 2) and serve as an estimation for the systematic errors due to extrapolation to low transverse momentum.

The bottom panel of Fig. 2 shows the rapidity dependence of the average transverse momentum $\langle p_T \rangle$ for pions and kaons. For pions, $\langle p_T \rangle \sim 0.41$ GeV/c at $y = 0$ and decreases to ~ 0.32 GeV/c at $y > 3.0$ while for kaons, $\langle p_T \rangle$ drops from ~ 0.65 GeV/c at $y = 0$ to ~ 0.5 GeV/c at $y = 3.2$. The drop of the averaged transverse momentum at forward rapidity is accompanied by a relatively large decrease in particle densities and in collective models can be explained by the decrease of the collective radial flow velocity.

Figure 3 shows the rapidity-dependent anti-hadron to hadron integrated yield ratios for pions, kaons and protons. The $\bar{p}/p$ ratios are obtained from the ratios of yields. The baryon yields are not corrected for feed-down from hyperons (see [23]). The π^-/π^+ ratio is approximately equal to unity over the entire rapidity range. The kaon and proton ratios at mid-rapidity ($K^-/K^+ \sim 0.85$, $\bar{p}/p \sim 0.45$) are lower than the corresponding ones measured at the top RHIC energy [22], but they are still characteristic of a high degree of anti-matter to matter equili-

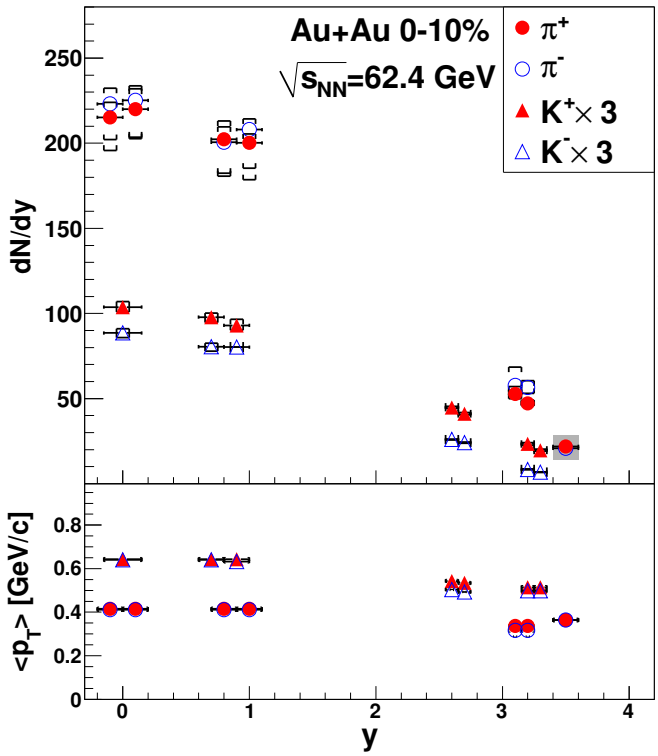

Figure 2: Upper panel: dN/dy as a function of rapidity for $\pi^{\pm}$ and $K^{\pm}$ from 0-10% central Au+Au collisions at $\sqrt{s_{NN}}$ = 62.4 GeV. The error bars are statistical. The square brackets below and above each data point indicate the dN/dy values extracted with the selected functionals (see Tables 1 and 2). The experimental uncertainties on the extrapolated yields are below 5% and not shown in the figure, except for the pion yields at y = 3.5 where these amount to ~ 30% and are indicated by the gray box. Bottom panel: $\langle p_T \rangle$ dependence on y. The error bars are statistical errors.

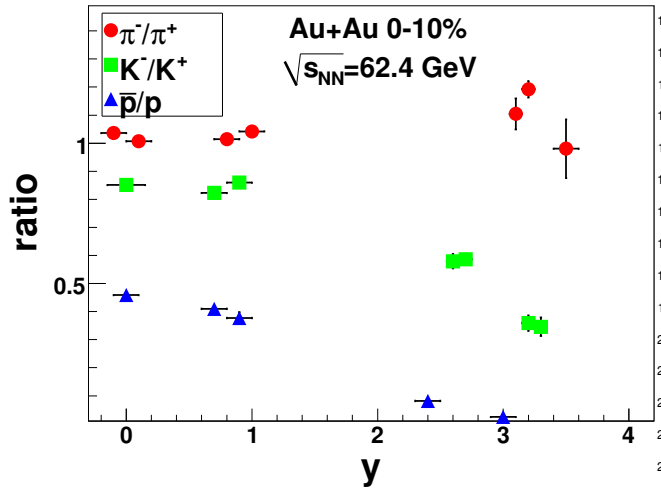

Figure 3: Anti-particle to particle ratios as a function of rapidity in 0-10% central Au+Au collisions at $\sqrt{s_{NN}}$ = 62.4 GeV. The error bars are statistical only.

bration. At forward rapidity we observe a decrease of the kaon ratio to a value of ~ 0.35 at y = 3.3. Possible explanations include the competition between Λ baryons and K^- mesons for the available strange quarks and associated production (e.g., $p + p \rightarrow p + \Lambda + K^+$) which increases the number of positive kaons. Both of these mechanisms depend on the net-baryon content and, consequently, lead to a decrease of the K^-/K^+ ratio at forward rapidity. The $\bar{p}/p$ ratio decreases significantly with rapidity, reaching $\bar{p}/p = 0.0818 \pm 0.0037(stat.)$ at y=2.4 and $\bar{p}/p = 0.0244 \pm 0.0010(stat.)$ at y = 3. The results are consistent within errors with those presented in [23].

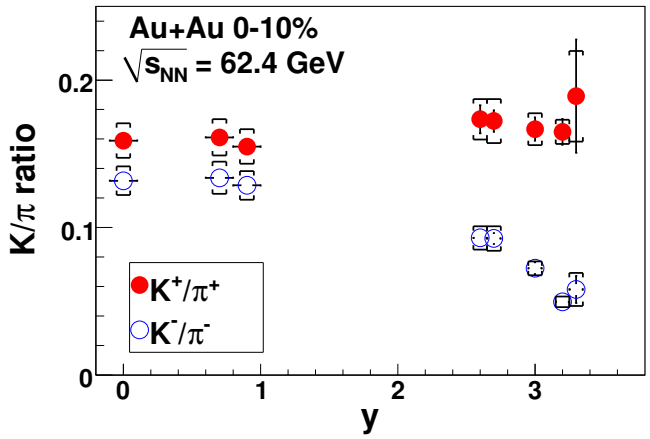

Figure 4: Rapidity dependence of the K/π ratios in 0-10% central Au+Au collisions at $\sqrt{s_{NN}}$ = 62.4 GeV. The error bars are statistical errors and the square brackets show the systematic uncertainties due to the yield extrapolation at low p_T.

In Fig. 4 we show the rapidity dependence of the K/π ratio. Because the rapidity intervals where the yields of the two species were extracted are not the same at forward rapidity, we used a linear interpolation procedure between the closest covered points to obtain the meson yields for additional points in rapidity. We checked this procedure by assuming Gaussian rapidity distributions and found very similar results. The K^+/π^+ ratio was found to be 0.159 ± 0.011 at mid-rapidity and is almost constant as a function of rapidity. The K^-/π^- ratio has a value of 0.132 ± 0.010 at mid-rapidity and shows a steep decrease for $y > 2.5$ with a value of ~ 0.05 at y = 3.2. The different rapidity dependence of the positive and negative charge K/π ratios is similar to, but somewhat more pronounced than that found in central Au+Au collisions at $\sqrt{s_{NN}}$ = 200 GeV [4].

In the following we use calculations with two microscopic transport models for comparison with our data. Ultra-Relativistic Quantum Molecular Dynamics (UrQMD) [18, 19] is the extension of RQMD [10, 11] which was developed to describe physics at AGS and SPS energies. At low energies, $\sqrt{s_{NN}} < 5$ GeV, it describes the nuclear collisions in terms of interactions between known hadrons and their resonances while at higher energies the dominant mechanism is the color string excitation. AMPT (A Multiphase Transport Model) [20, 21] is a microscopic model developed for nucleus-nucleus collisions at RHIC and LHC energies. AMPT uses the HIJING model for

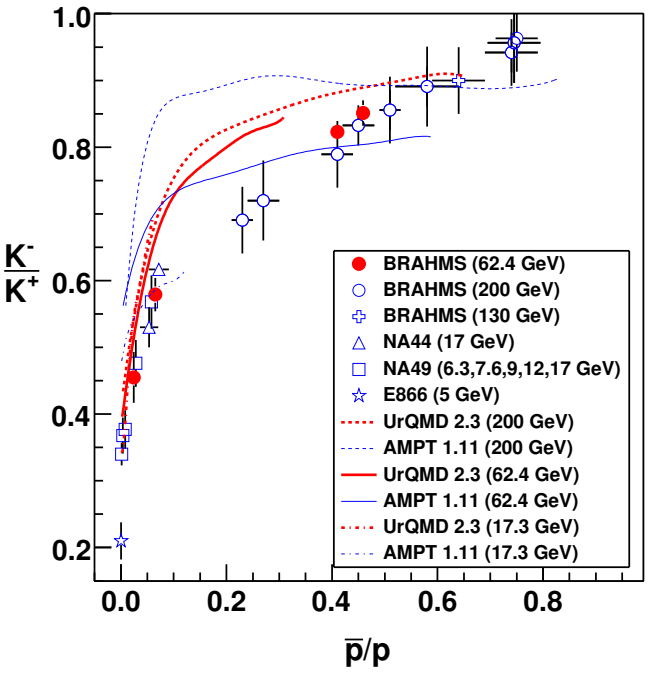

Figure 5: (Color online) K^-/K^+ ratio dependence on the $\bar{p}/p$ ratio. The solid circles are from 0-10% central Au+Au collisions at $\sqrt{s_{NN}}$ = 62.4 GeV obtained in the present work. The open symbols are BRAHMS data from ref. [22] and lower energy data from [3, 26, 27, 28, 29, 30]. The error bars represent statistical and systematic errors. The curves are calculations with UrQMD (thick red lines) and AMPT (thin blue lines) for central Au+Au collisions at $\sqrt{s_{NN}}$=200 GeV (dashed lines) and 62.4 GeV (solid lines) and for central Pb+Pb collisions at $\sqrt{s_{NN}}$=17.3 GeV (dot-dashed lines).

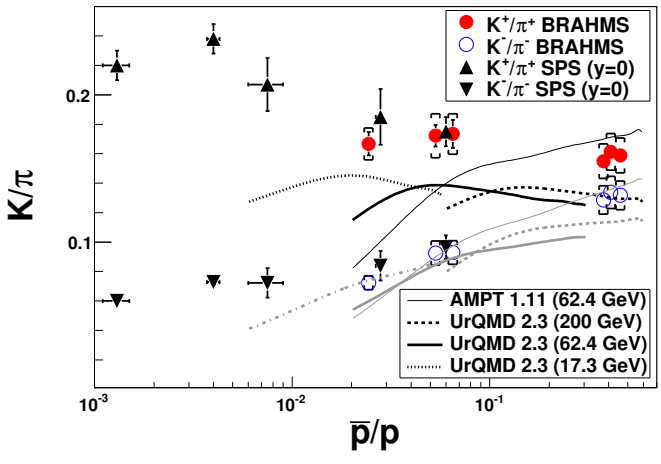

Figure 6: (Color online) K/π ratios as functions of the $\bar{p}/p$ ratio. The circles are data from 0-10% central Au+Au collisions at $\sqrt{s_{NN}}$ = 62.4 GeV and the triangles are results measured at mid-rapidity in the SPS experiments at different energies [13]. The curves are UrQMD (thick lines) and AMPT (thin lines) calculations for central Au+Au collisions at $\sqrt{s_{NN}}$ = 17.3, 62.4 and 200 GeV. The black curves are for the K^+/π^+ ratio and gray curves are for the K^-/π^- ratio.

the initial space-time configuration of the partons and strings. Both UrQMD and AMPT include a Lund-type string fragmentation procedure followed by hadronic rescatterings. The models were run in minimum bias mode with a 0-10% centrality cut placed on the distribution of particles falling in the acceptance of our multiplicity detector ($|\eta| < 2.2$), closely mimicking the experimental conditions.

Figure 5 shows the dependence of the K^-/K^+ ratio on the $\bar{p}/p$ ratio in central nucleus-nucleus collisions at energies ranging from $\sqrt{s_{NN}}$ = 5 GeV to $\sqrt{s_{NN}}$ = 200 GeV. The data points obtained in this work and from the other RHIC energies are obtained in different rapidity slices, while the SPS and AGS points are obtained at mid-rapidity. Comparing the low and high energy results, we observe a systematic dependence of the K^-/K^+ ratio on the $\bar{p}/p$ ratio. The calculations made with UrQMD(thick lines) and AMPT(thin lines) for central nucleus-nucleus collisions at $\sqrt{s_{NN}}$ = 200, 62.4 and 17.3 GeV do not reproduce the dependence of the K^-/K^+ ratio on the $\bar{p}/p$ ratio which seems to be universal over a large energy range. However, UrQMD calculations at the three energies give similar K^-/K^+ ratios in the common interval of $\bar{p}/p$ values.This is most likely due to the thermalization of the system reached via secondary rescatterings, which includes formation, decay and regeneration of many resonances [31].

Figure 6 shows the dependence of the K/π ratios on the $\bar{p}/p$ ratio. Our data points are obtained in different rapidity slices at the same energy, $\sqrt{s_{NN}}$ = 62.4 GeV, while the SPS points are obtained at mid-rapidity in central Pb+Pb collisions at $\sqrt{s_{NN}}$ = 6.3, 7.6, 8.8, 12.3 and 17.3 GeV. In Au+Au collisions at 62.4 GeV, the fragmentation peak is estimated to be in the interval $2.5 < y < 3.3$ [23] with a net-proton density of ~ 30 and $\bar{p}/p$ ratio values at forward rapidity in the same range as the ones measured at mid-rapidity at $\sqrt{s_{NN}}$ = 12.3 and 17.3 GeV. As in the case of K^-/K^+ ratio, we observe there is a smooth dependence of the K/π ratios on the $\bar{p}/p$ ratio. The curves show calculations for central Au+Au collisions from UrQMD (thick lines) at $\sqrt{s_{NN}}$ = 17.3, 62.4 and 200 GeV and AMPT (thin lines) at $\sqrt{s_{NN}}$ = 62.4 GeV. None of the models reproduce the dependence of the K/π ratios on the $\bar{p}/p$ ratio.

The inverse slope of the spectra for positive and negative kaons measured at forward rapidity in our dataset are ~ 20 MeV smaller than the ones measured at mid-rapidity in SPS experiments at the same $\bar{p}/p$ ratio, albeit almost consistent within the error bars (see Fig. 7). The difference in inverse slopes might also be due to the radial flow velocity which is expected to depend on the local system size and multiplicity. The three equal inverse slopes obtained at $0 < y < 1$ are the result of a simultaneous fit to the spectra giving just a single value.

In a chemical analysis, the $\bar{p}/p$ ratio has an approximate correspondence with the baryo-chemical potential through the formula $\bar{p}/p = \exp(-2\mu_B/T)$ for a given freeze-out temperature T. Hence if T is the same in the two cases, this would imply that the local system formed at high rapidity at RHIC (62.4 GeV) is chemically equivalent with the system formed at the two highest SPS energies at mid-rapidity, both being controlled by the baryo-chemical potential. The strangeness chemical potential is fixed by the baryo-chemical potential and chemical freeze-out

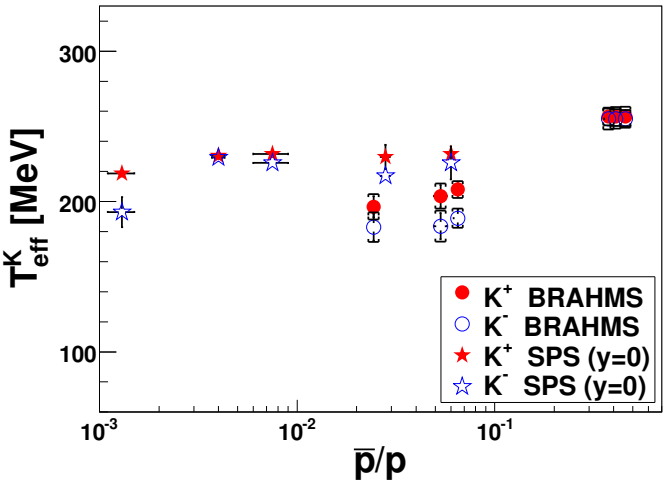

Figure 7: Inverse slopes ($T_{\rm eff}$) for kaons as a function of the $\bar{p}/p$ ratio. The BRAHMS points are from 0-10% central Au+Au collisions at $\sqrt{s_{NN}}$ = 62.4 GeV (this analysis) at different rapidities while the SPS points are from mid-rapidity at different energies [13]. The three equal inverse slopes obtained at $0 < y < 1$ are the result of a simultaneous fit to the spectra giving just a single value. The error bars represent statistical errors, while the square brackets show systematic errors.

temperature provided that the local net strangeness vanishes. A rapidity dependent baryo-chemical potential μ_B has been suggested in thermal models [24, 25]. The observed dependence of the chemical freeze-out composition in different colliding systems and different rapidities only on the baryo-chemical potential and temperature supports the idea of local chemical equilibration and the existence of a universal ($T - \mu_B$) freeze-out line.

Summary

In summary, we have measured the transverse momentum spectra and inclusive invariant yields of charged pions and kaons in central Au+Au reactions at 62.4 GeV. The anti-particle/particle ratios for kaons and protons show a steep decrease at forward rapidity. The rapidity dependence of the K/π ratio depends on charge, which is understood in microscopical models (*i.e.* UrQMD) as resulting from the associated production mechanisms in a baryon rich medium, which enhance the fraction of s quarks ending up in hyperons, thus depleting the K^- yield. We observe in central nucleus-nucleus collisions a common dependence of the particle ratios (K/π, K^-/K^+) and kaon spectra inverse slopes on the baryo-chemical potential, whether measured for different energies at mid-rapidity at SPS, or at different rapidities at $\sqrt{s_{NN}}$ = 62.4 GeV. This is consistent with a picture where in nucleus-nucleus collisions, at a given energy, the local fireballs formed at different rapidities freeze out on a $T - \mu_B$ line which coincide with the $T - \mu_B$ freeze-out line previously observed in a wide energy range but only at mid-rapidity. The baryo-chemical potential interval covered at forward rapidity extends to high values and is equivalent to the two highest SPS energies, but not quite high enough to probe the horn structure in the K^+/π^+ ratio excitation function. In the calculations made with UrQMD and AMPT models, K/π ratios are not well reproduced for large baryo-chemical potential found either at high rapidity or mid-rapidity at lower energies. Also, the universal dependence of the K^-/K^+ on the $\bar{p}/p$ ratio is not well explained by these microscopic transport models.

Acknowledgements

This work was supported by the Division of Nuclear Physics of the Office of Science of the U.S. Department of Energy under contracts DE-AC02-98-CH10886, DE-FG03-93-ER40773, DE-FG03-96-ER40981, and DE-FG02-99-ER41121, the Danish Natural Science Research Council, the Research Council of Norway, the Polish Ministry of Science and Higher Education under grant N N202 124836, and the Romanian Ministry of Education and Research (5003/1999, 6077/2000). We thank the staff of the Collider-Accelerator Division at BNL and the RHIC Computing Facility for their support to the experiment.

References

[1] L. Ahle *et al.*, E802 Coll., *Phys.Rev.* **C57** (1998) 466
[2] L. Ahle *et al.*, E802 Coll., *Phys.Rev.* **C58** (1998) 3523
[3] S.V. Afanasiev *et al.*, NA49 Coll., *Phys.Rev.* **C66** (2002) 054902
[4] I.G. Bearden *et al.*, BRAHMS Coll., *Phys.Rev.Lett.* **94** (2005) 162301
[5] L. Ahle *et al.*, E802 Coll., *Phys.Rev.* **C59** (1999) 2173
[6] C. Alt *et al.*, NA49 Coll., *Phys.Rev.* **C73** (2006) 044910
[7] I.G. Bearden *et al.*, BRAHMS Coll., *Phys.Rev.Lett.* **93** (2004) 102301
[8] L. Ahle *et al.*, E866 and E917 Coll., *Nucl.Phys.* **A638** (1998) 57C
[9] S. Ahmad *et al.*, E891 Coll., *Phys.Lett.* **B382** (1996) 35
[10] H. Sorge, H. Stöcker and W. Greiner, *Ann.Phys. (NY)* **192** (1989) 266
[11] H. Sorge, H. Stöcker and W. Greiner, *Nucl.Phys.* **A498** (1989) 567
[12] M. Gazdzicki and M. Gorenstein, *Acta Phys.Polon.* **B30** (1999) 2705
[13] M. Mitrovski *et al.*, NA49 Coll., *J.Phys.* **G32** (2006) S43
[14] I. Arsene *et al.*, BRAHMS Coll., *Nucl.Phys.* **A757** (2005) 1
[15] M. Adamczyk *et al.*, BRAHMS Coll., *Nucl.Instr.Meth.* **A499** (2003) 437
[16] R. Debbe *et al.*, *Nucl.Instr.Meth.* **A570** (2007) 216
[17] B.B. Back *et al.*, PHOBOS Coll., *Phys.Rev.* **C77** (2007) 024910
[18] S.A. Bass *et al.*, *Prog.Part.Nucl.Phys.* **41** (1998) 225
[19] M. Bleicher *et al.*, *J.Phys.* **G25** (1999) 1859
[20] B. Zhang *et al.*, *Phys.Rev.* **C61** (2000) 067901
[21] Z.-w. Lin *et al.*, *Nucl.Phys.* **A698** (2002) 375
[22] I.G. Bearden *et al.*, BRAHMS Coll., *Phys.Rev.Lett.* **90** (2003) 10
[23] H. Dalsgaard *et al.*, BRAHMS Coll., *Int.J.Mod.Phys.* **E16** (2007) 7; I.C. Arsene *et al.*, BRAHMS Coll., *Phys.Lett.* **B677** (2009) 267
[24] F. Becattini, J.Cleymans, *J.Phys.* **G34** (2007) S959
[25] B. Biedron, W. Broniowski, *J.Phys.* **G35** (2008) 044011; *Phys.Rev.* **C76** (2007) 054905
[26] L. Ahle *et al.*, E866 Coll., *Phys.Rev.Lett.* **81** (1998) 2650
[27] M.van Leeuwen *et al.*, NA49 Coll., *Nucl.Phys.* **A715** (2003) 161
[28] C. Alt *et al.*, NA49 Coll., *Phys.Rev.* **C77** (2008) 024903
[29] C. Alt *et al.*, NA49 Coll., *Phys.Rev.* **C73** (2006) 044910
[30] I.G. Bearden *et al.*, NA44 Coll., *Phys.Rev.* **C66** (2002) 044907
[31] L. V. Bravina *et al.*, *Phys.Rev.* **C78** (2008) 014907